JETIR.ORG ISSN: 2349-5162 | ESTD Year : 2014 | Monthly Issue
JOURNAL OF EMERGING TECHNOLOGIES AND INNOVATIVE RESEARCH (JETIR)
An International Scholarly Open Access, Peer-reviewed, Refereed Journal

MECHANICAL CHARACTERIZATION AND TESTING OF MULTI-MATERIAL POLYMER COMBINATION IN 3D PRINTING TECHNOLOGY

Taguchi L9 optimization of a tri-fibre PETG-CF / ASA / PETG laminate printed by multi-nozzle FDM

[1]Priya S, [2]Dr. S. Somasundaram
[1]PG Scholar (M.Tech Mechatronics), [2]Professor and Head
[1,2]Department of Mechanical Engineering,
[1,2]National Institute of Technical Teachers Training and Research (NITTTR), Chennai, India

Abstract : Additive manufacturing (AM) is receiving increasing attention because it enables cost- and resource-efficient small-scale production of complex parts. This work characterizes the mechanical behaviour of a tri-fibre laminate produced on a newly developed five-nozzle fused deposition modelling (FDM) printer, in which PETG-CF, ASA and PETG filaments are deposited in separate layer stacks within a single specimen. Three process parameters, layer height (0.15, 0.20, 0.30 mm), printing speed (30, 50, 70 mm/s) and infill density (20, 25, 30 %), were varied using a Taguchi L9 orthogonal array and the responses impact energy, tensile strength, compressive strength and flexural load were measured. Signal-to-noise (S/N) analysis and ANOVA in Minitab 17 show that printing speed is the dominant factor for tensile (56 %) and compressive (48 %) strength while layer height dominates impact energy (49 %); flexural load is insensitive to the chosen process window. The best trial values were 30.12 N/mm² tensile strength, 26.41 N/mm² compressive strength, 3.43 J impact energy and 0.29 kN flexural load. Compared with mono-material specimens, the tri-fibre laminate exceeded PETG-CF, ASA and PETG in compressive strength and impact energy, nearly matched PETG-CF in tensile strength and fell short of PETG-CF in flexural load. Peak tensile strength is associated with the largest PETG fraction, while the largest ASA fraction favours compressive and flexural performance.

IndexTerms - Fused deposition modelling, multi-nozzle extruder, PETG-CF, ASA, PETG, Taguchi method, ANOVA, mechanical characterization.

I. INTRODUCTION

Additive manufacturing builds a component from a 3D CAD model by adding material layer upon layer, in contrast to subtractive processes such as machining and stamping that remove material from a larger stock. AM generates very little waste, needs no dedicated tooling or fixtures, and can realise intricate geometries and consolidated assemblies that are difficult or impossible to produce by conventional means. Since its origin in the 1980s the technology has advanced rapidly and now supports customised healthcare products, reduced material and energy consumption, and on-demand manufacturing with shorter supply chains.

Fused deposition modelling (FDM), also called fused filament fabrication (FFF), is the most widely used material-extrusion AM process. A thermoplastic filament is driven into a heated nozzle and extruded onto a build platform one layer at a time. FDM is inexpensive, fast and compatible with many polymers (ABS, PLA, PETG, nylon), but parts exhibit comparatively low resolution, rough surfaces and anisotropic strength because of the weak interface between adjacent layers. The mechanical behaviour of an FDM part is therefore strongly governed by process parameters such as layer height, printing speed, nozzle and bed temperature, infill density, infill pattern, build orientation, raster angle and raster width.

Rapid prototyping parts often suffer from poor mechanical properties, and composite reinforcement is one of the recognised remedies. Fibre reinforcement can be introduced into FDM through a pre-compounded composite filament, by impregnation inside the nozzle, or by feeding the fibre after the nozzle. A conventional single-extruder printer, however, can process only one filament at a time and any material change requires the print to be paused, the chamber cleaned and a new filament loaded. Multi-nozzle extruders overcome this limitation by keeping several filaments loaded simultaneously, enabling multi-material and multi-colour parts, faster printing and dedicated support material.

In the present study a first-of-its-kind five-nozzle FDM printer was developed. The hot section carries five nozzles on a circular holding plate, each with its own heater and thermistor; the cold section feeds and switches filaments with only three stepper motors, keeping the head light and fast in all three axes. Using this machine, tri-fibre specimens of PETG-CF, ASA and PETG were printed in stacked layers and their impact, tensile, compressive and flexural behaviour was characterised. The Taguchi method with an L9 orthogonal array was employed to identify the most influential printing parameters and their optimum levels, and the laminate was benchmarked against each constituent filament printed alone.

II. LITERATURE REVIEW

Kim et al. [1] conducted tensile tests on single- and dual-material 3D printed products and showed that structural arrangement and material ratio govern the effectiveness of dual-material prints. Arigela and Vikram Kumar [2] mounted a dual-nozzle extruder on an industrial robot and reported stronger interlayer bonding through extruder re-orientation together with reduced print time. Daramwar and Kadam [3] reviewed multi-material extrusion mechanisms, including cam-operated movable hot ends, dual hot-end lifting and multiple printing heads, and concluded that multiple heads give the most efficient and accurate multi-material printing.

Giri et al. [4] optimised layer thickness, air gap, raster width, build orientation, raster angle and number of contours for a dual-extruder PLA printer using an artificial neural network, achieving correlation coefficients above 0.998 for tensile strength, build time and surface roughness. Issayev [5] printed PLA, ABS and flexible specimens with 10, 25 and 100 % infill on a multi-extrusion printer and found that the bond strength of single, dual and triple material specimens depended on the reinforcement strategy. Sunil Kumar [6] designed a low-cost dual-extruder machine with a heated dual-nozzle system and cooling platform, while Shojaie et al. [7] demonstrated the feasibility of dual-nozzle FDM for a bicompartmental colon-targeted drug-delivery device.

Szczęch and Sikora [8] related layer height and temperature to leakage and strength of PLA vessels and found that a smaller layer height improved both tightness and strength, with temperature having a smaller effect. Wang et al. [9] showed that 5 wt.% carbon fibre markedly stiffens PLA and ranked the influence of parameters on tensile strength as layer thickness > bed temperature > printing speed > nozzle temperature, with an optimum at 0.1 mm, 60 °C, 40 mm/s and 215 °C. Alkabbanie et al. [10] reported that lower layer height raised flexural and impact strength of short-CF PLA by about 28 %, that higher feed rate improved strength by about 12.6 %, and that higher extrusion temperature improved impact but reduced flexural strength. Kaushik et al. [11] and Pérez Mendoza et al. [12] examined tensile, flexural, wear and impact behaviour of CF-reinforced PLA at different infill percentages, and Li et al. [13] characterised the compressive response of 3D-printed polyurethane acrylate elastomer lattices.

The literature therefore establishes that multi-nozzle FDM is feasible and that carbon-fibre reinforcement and process parameters strongly affect mechanical properties. Systematic Taguchi-based optimisation of a three-material PETG-CF/ASA/PETG laminate printed on a multi-nozzle machine has, however, not been reported, and this gap is addressed here.

III. MATERIALS AND METHODS

3.1 Filament materials

PETG (glycol-modified polyethylene terephthalate) was chosen for its high strength, low shrinkage and excellent layer adhesion. PETG-CF contains short carbon fibres that give roughly three times the tensile modulus and twice the tensile strength of plain PETG, at the cost of lower impact resistance; it is preferred for structural parts, functional prototypes and machine components. ASA (acrylonitrile styrene acrylate) is compositionally similar to ABS but was developed for superior UV and weather resistance, with high dimensional stability and good chemical resistance. The printing conditions used for the three filaments are summarised in Table 1.

Table 1. Printing conditions of the filaments

Property	PETG	PETG-CF	ASA
Filament diameter (mm)	1.75	1.75	1.75
Density (g/cc)	1.27	–	–
Nozzle temperature (°C)	235	235 (brass/hardened nozzle)	220–250
Bed temperature (°C)	60	60	90–110

3.2 Multi-nozzle FDM printer

The specimens were printed on the newly developed five-nozzle FDM machine. The extrusion system consists of a hot section with five nozzles fixed through thermal barriers to a circular holding plate, each nozzle having an individual heater and temperature sensor, and a cold section that feeds the filament through a spring-loaded gear driven by a stepper motor. A second stepper motor with proximity sensors indexes the required nozzle and a third light motor engages the feed gear. Because all filaments remain loaded, no manual filament change is required, which reduces print time, maintenance and cleaning. The remaining components are the frame, heated build platform, control electronics and power supply of a standard FDM printer.

3.3 Specimen construction

Each specimen was built as a stacked laminate of PETG-CF (black), ASA (brown) and PETG (white). The layer stack thickness of each material was varied between trials so that the total specimen thickness remained constant, as listed in Table 2. Fusion temperature and infill pattern were held constant and specimens for tensile, compressive, flexural and impact testing were printed under the same parameters.

Table 2. Thickness (mm) and number of layers of each material in the laminate

Trial	PETG-CF thick.	Layers	ASA thick.	Layers	PETG thick.	Layers
1	1	22	2	44	0.5	12
2	2	44	0.5	12	1	22
3	0.5	12	1	22	2	44
4	1	22	0.5	12	2	44
5	0.5	12	2	44	1	22
6	2	44	1	22	0.5	12

Trial	PETG-CF thick.	Layers	ASA thick.	Layers	PETG thick.	Layers
7	1.5	18	1	22	1	12
8	1	12	1	12	1.5	18
9	1	12	1.5	18	1	12

IV. EXPERIMENTAL DESIGN

4.1 Taguchi method

Classical factorial designs require a large number of experiments as the number of factors grows. The Taguchi method instead uses a special orthogonal array to examine the whole parameter space with few runs. The experimental results are converted into a signal-to-noise (S/N) ratio that measures the deviation of the quality characteristic from its desired value; a larger S/N ratio always indicates better quality, so the optimum level of each parameter is the level with the highest S/N ratio. Since all four responses are to be maximised, the larger-is-better criterion was used:

$$S/N = -10 \log_{10} \left[(1/n) \Sigma (1/Y_i^2) \right] \quad (1)$$

where Y is the measured response and n the number of observations. Analysis of variance (ANOVA) was then applied to the raw responses to quantify the percentage contribution of each parameter to the total variation.

4.2 Parameters, levels and orthogonal array

Three process parameters were studied at three levels each (Table 3) and the experiments were arranged in a standard L9 (3^3) orthogonal array generated in Minitab 17 (Table 4). Impact energy (Charpy, J), tensile strength (N/mm²), compressive strength (N/mm²) and flexural load (kN) were recorded for each run; the complete experimental data are given in Table 4.

Table 3. Process parameters and their levels

Level	Layer height (mm)	Printing speed (mm/s)	Infill density (%)
1	0.15	30	20
2	0.20	50	25
3	0.30	70	30

Table 4. L9 orthogonal array and measured responses

Trial	Layer height (mm)	Printing speed (mm/s)	Infill density (%)	Impact energy (J)	Tensile strength (N/mm²)	Comp. strength (N/mm²)	Flexural load (kN)
1	0.15	30	20	2.94	28.15	20.47	0.26
2	0.15	50	25	2.84	25.93	20.00	0.23
3	0.15	70	30	3.33	30.12	24.53	0.25
4	0.20	30	25	3.04	24.44	20.47	0.24
5	0.20	50	30	2.74	25.19	21.88	0.29
6	0.20	70	20	2.94	27.90	21.72	0.22
7	0.30	30	30	3.43	22.42	24.06	0.24
8	0.30	50	20	3.23	24.20	20.00	0.27
9	0.30	70	25	3.17	28.15	26.41	0.24

V. RESULTS AND DISCUSSION

5.1 Variation of responses across the L9 trials

Fig. 1 plots the four measured responses against trial number. Impact energy ranged from 2.74 J (trial 5) to 3.43 J (trial 7), tensile strength from 22.42 N/mm² (trial 7) to 30.12 N/mm² (trial 3), compressive strength from 20.00 N/mm² (trials 2 and 8) to 26.41 N/mm² (trial 9), and flexural load from 0.22 kN (trial 6) to 0.29 kN (trial 5). The highest impact energy was obtained in trial 7 at the maximum layer height, lowest printing speed and highest infill, with a comparatively large PETG-CF fraction. Peak tensile strength (trial 3) occurred at the minimum layer height, highest printing speed and highest infill, where the PETG fraction was largest. Peak compressive strength (trial 9) and flexural load (trial 5) were associated with the largest ASA fraction in the laminate.

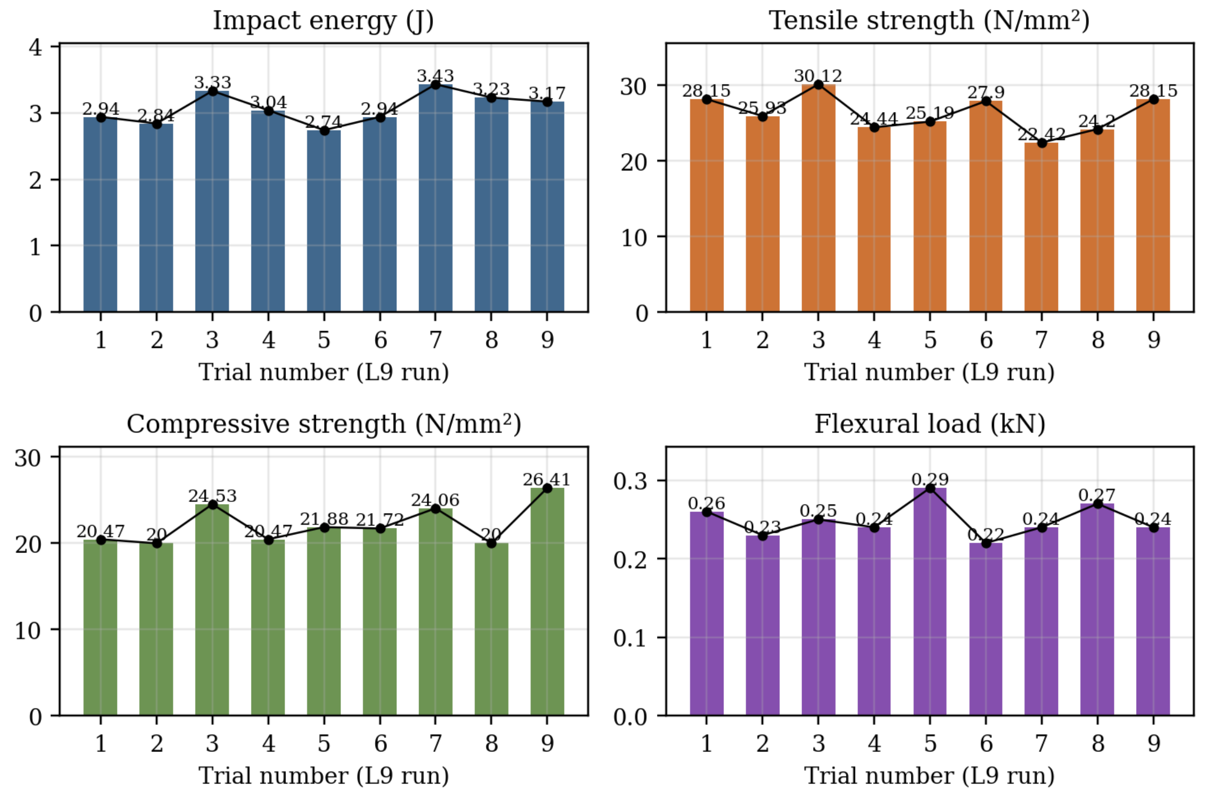

Fig. 1. Measured impact energy, tensile strength, compressive strength and flexural load for the nine L9 trials

5.2 Signal-to-noise analysis

Table 5 lists the S/N ratios computed with Eq. (1) and the resulting response tables (mean S/N ratio at each level, delta and rank) are given in Table 6. Fig. 2 shows the corresponding main-effects plots. For impact energy, layer height has the largest delta (1.044 dB) and the S/N ratio is highest at 0.30 mm, 70 mm/s and 30 % infill. For tensile strength, printing speed ranks first (delta 1.24 dB), with the best S/N at 0.15 mm, 70 mm/s and 20 % infill; tensile strength falls monotonically as layer height increases, consistent with better inter-layer fusion of thinner layers. Compressive strength is likewise governed by printing speed (delta 1.37 dB) followed by infill density (1.08 dB), and is maximised at 0.30 mm, 70 mm/s and 30 %. Flexural load shows very small deltas for all factors (≤ 0.90 dB) and its nominal optimum is 0.30 mm, 50 mm/s and 30 % infill.

Table 5. S/N ratios (larger-is-better) of the measured responses

Trial	S/N impact (dB)	S/N tensile (dB)	S/N compressive (dB)	S/N flexural (dB)
1	9.3669	27.9762	26.2224	−11.7005
2	9.0664	27.2647	26.0206	−12.7654
3	10.4489	28.5659	27.7940	−12.0412
4	9.6575	26.7532	26.2224	−12.3958
5	8.7550	27.0127	26.8009	−10.7520
6	9.3669	27.9030	26.7372	−13.1515
7	10.7059	27.0127	27.6259	−12.3958
8	10.1841	26.6649	26.0206	−11.3727
9	10.0212	27.9762	28.4354	−12.3958

Table 6. Response tables for S/N ratios (LH = layer height, PS = printing speed, ID = infill density)

Response	Level	LH	PS	ID
Impact energy	1	9.627	9.910	9.639
	2	9.260	9.335	9.582
	3	10.304	9.946	9.970
	Delta / Rank	1.044 / 1	0.611 / 2	0.388 / 3
Tensile strength	1	28.95	27.92	28.53
	2	28.23	27.99	28.34
	3	27.89	29.16	28.20
	Delta / Rank	1.05 / 2	1.24 / 1	0.32 / 3
Compressive strength	1	26.68	26.69	26.33
	2	26.59	26.28	26.89
	3	27.36	27.66	27.41
	Delta / Rank	0.77 / 3	1.37 / 1	1.08 / 2

Response	Level	LH	PS	ID
Flexural load	1	−12.17	−12.16	−12.07
	2	−12.10	−11.63	−12.52
	3	−12.05	−12.53	−11.73
	Delta / Rank	0.11 / 3	0.90 / 1	0.79 / 2

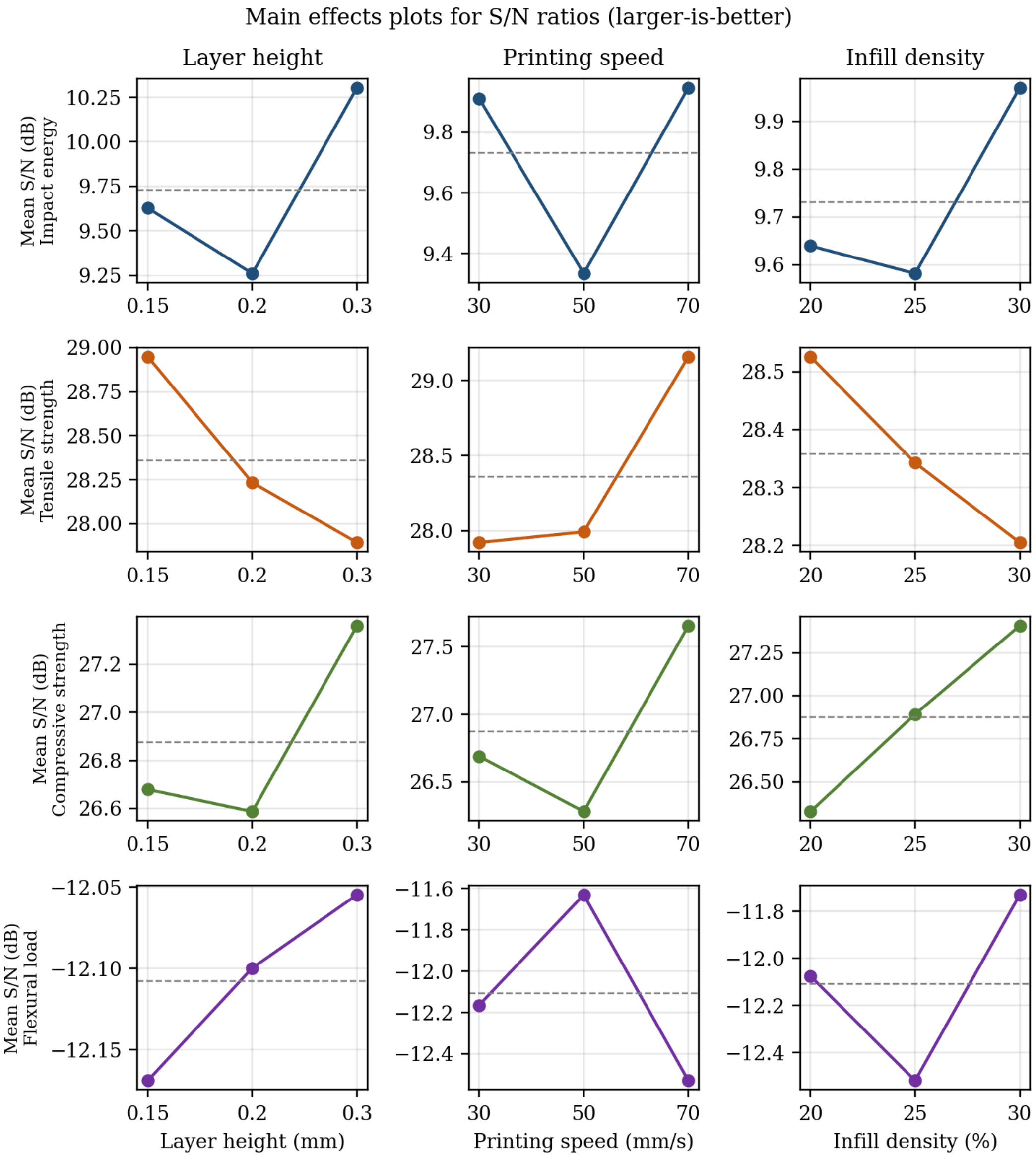

Fig. 2. Main effects plots for S/N ratios of impact energy, tensile strength, compressive strength and flexural load

The main-effects plots for means (Fig. 3) confirm the same trends on the original scale: mean impact energy rises from 2.91 J at 0.20 mm to 3.28 J at 0.30 mm layer height; mean tensile strength increases from 25.0 N/mm² at 30 mm/s to 28.7 N/mm² at 70 mm/s and decreases from 28.1 N/mm² at 0.15 mm to 24.9 N/mm² at 0.30 mm; mean compressive strength rises from 20.6 N/mm² at 50 mm/s to 24.2 N/mm² at 70 mm/s and from 20.7 N/mm² at 20 % infill to 23.5 N/mm² at 30 %. Mean flexural load varies by only 0.027 kN over the entire design.

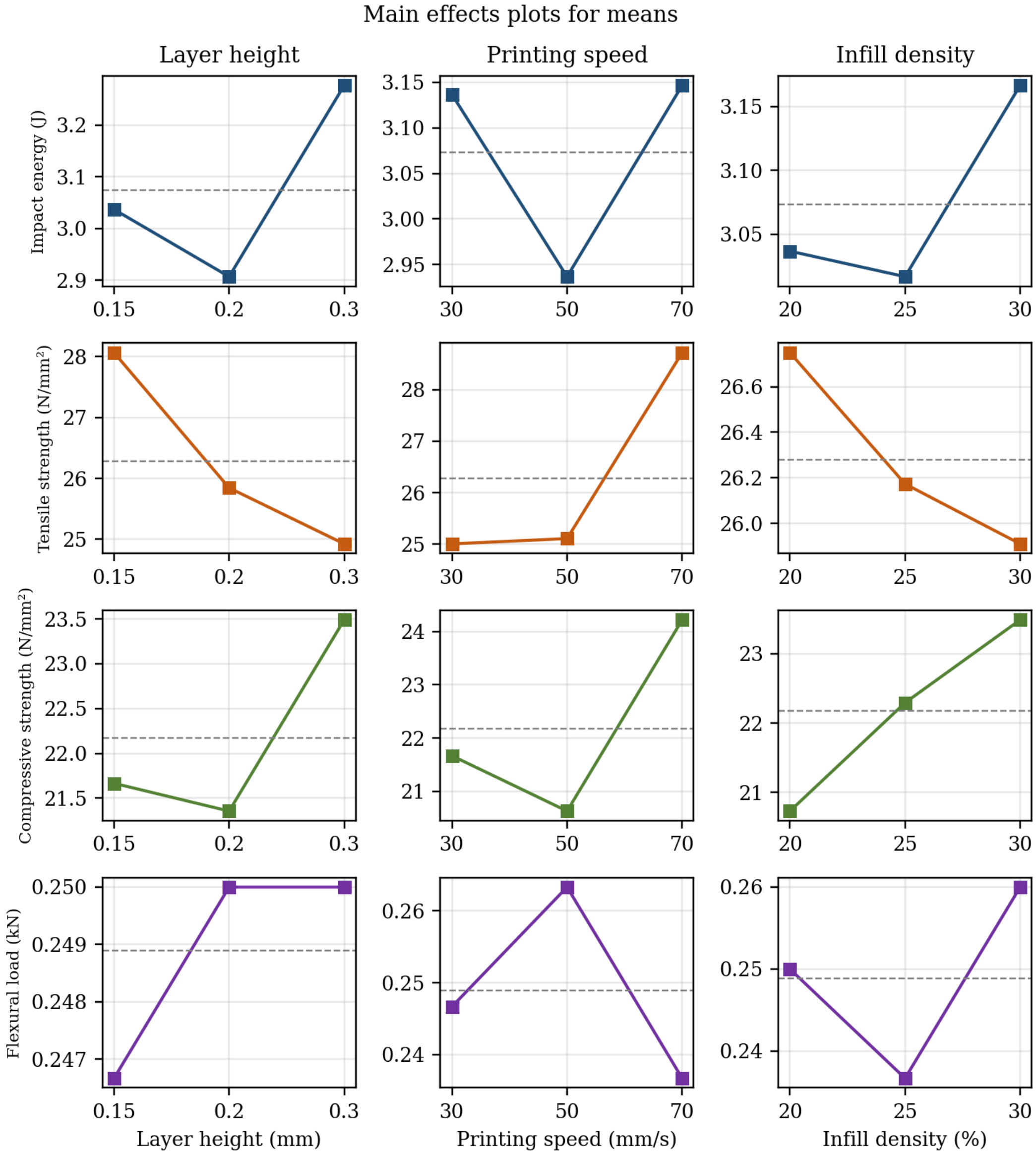

Fig. 3. Main effects plots for means of the four responses

5.3 Analysis of variance

The ANOVA results obtained from the general linear model in Minitab 17 are summarised in Table 7 and the percentage contributions are compared in Fig. 4. Layer height contributes 49 % of the variation in impact energy, printing speed 20 % and infill density 9 %. For tensile strength printing speed contributes 56 % and layer height 33 %, with infill density practically inert (2 %) and a residual error of only 9 % (R^2 = 90.5 %). Compressive strength gives the best-fitting model (R^2 = 93.8 %, error 6 %) with printing speed at 48 %, infill density 27 % and layer height 19 %. For flexural load the error term accounts for 48 % (R^2 = 52 %) and layer height contributes essentially nothing, indicating that flexural behaviour is controlled by the laminate stacking and the PETG-CF fraction rather than by the selected process window.

With nine runs and only two degrees of freedom for error, no factor reaches the conventional 5 % significance level for any response; the smallest p-value is 0.113 for printing speed on compressive strength. Engineering significance is therefore judged from the delta values, rank order and percentage contribution, and confirmation experiments with replication are recommended before the optimum settings are adopted in production.

Table 7. ANOVA results and percentage contribution of the process parameters

Response	Source	DF	Adj SS	Adj MS	F	p	Contribution (%)
Impact energy	Layer height	2	0.2114	0.1057	2.25	0.307	49
	Printing speed	2	0.0842	0.0421	0.90	0.527	20
	Infill density	2	0.0398	0.0199	0.42	0.702	9
	Error	2	0.0938	0.0469			22
Tensile strength	Layer height	2	15.670	7.835	3.42	0.226	33
	Printing speed	2	26.929	13.465	5.88	0.145	56
	Infill density	2	1.107	0.554	0.24	0.805	2
	Error	2	4.579	2.290			9
Compressive strength	Layer height	2	7.972	3.986	3.04	0.248	19
	Printing speed	2	20.513	10.257	7.81	0.113	48

Response	Source	DF	Adj SS	Adj MS	F	p	Contribution (%)
	Infill density	2	11.494	5.747	4.38	0.186	27
	Error	2	2.625	1.313			6
Flexural load	Layer height	2	0.000022	0.000011	0.01	0.988	≈0
	Printing speed	2	0.001089	0.000544	0.62	0.617	30
	Infill density	2	0.000822	0.000411	0.47	0.681	22
	Error	2	0.001756	0.000878			48

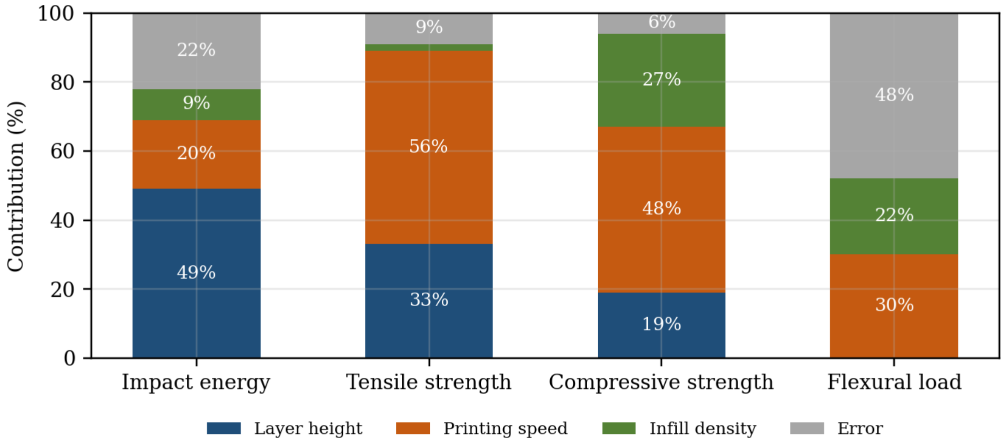

Fig. 4. Percentage contribution of layer height, printing speed and infill density to each response

5.4 Optimum parameter levels and regression models

The optimum levels identified from the S/N response tables are collected in Table 8 together with the response predicted by the fitted general linear model. The regression equations obtained in Minitab (factor coding −1, 0, +1) are:

$IE = 3.0733 - 0.037\,LH_{0.15} - 0.167\,LH_{0.20} + 0.203\,LH_{0.30} + 0.063\,PS_{30} - 0.137\,PS_{50} + 0.073\,PS_{70} - 0.037\,ID_{20} - 0.057\,ID_{25} + 0.093\,ID_{30}$

$TS = 26.278 + 1.789\,LH_{0.15} - 0.434\,LH_{0.20} - 1.354\,LH_{0.30} - 1.274\,PS_{30} - 1.171\,PS_{50} + 2.446\,PS_{70} + 0.472\,ID_{20} - 0.104\,ID_{25} - 0.368\,ID_{30}$

$CS = 22.171 - 0.504\,LH_{0.15} - 0.814\,LH_{0.20} + 1.319\,LH_{0.30} - 0.504\,PS_{30} - 1.544\,PS_{50} + 2.049\,PS_{70} - 1.441\,ID_{20} + 0.122\,ID_{25} + 1.319\,ID_{30}$

$FL = 0.24889 - 0.0022\,LH_{0.15} + 0.0011\,LH_{0.20} + 0.0011\,LH_{0.30} - 0.0022\,PS_{30} + 0.0144\,PS_{50} - 0.0122\,PS_{70} + 0.0011\,ID_{20} - 0.0122\,ID_{25} + 0.0111\,ID_{30}$

Table 8. Optimum process parameter levels and predicted responses

Response	Layer height (mm)	Printing speed (mm/s)	Infill density (%)	Dominant factor	Predicted value	R^2 (%)
Impact energy	0.30	70	30	Layer height (49 %)	≈ 3.45 J	78.2
Tensile strength	0.15	70	20	Printing speed (56 %)	≈ 31.0 N/mm²	90.5
Compressive strength	0.30	70	30	Printing speed (48 %)	≈ 26.9 N/mm²	93.8
Flexural load	0.30	50	30	None significant	≈ 0.27 kN	52.4

The two strength responses point in opposite directions with respect to layer height: tensile strength prefers thin 0.15 mm layers, whereas impact energy and compressive strength prefer thick 0.30 mm layers. High printing speed (70 mm/s) is beneficial for all three, so a compromise setting of 70 mm/s with 30 % infill and an intermediate layer height would be appropriate where several properties must be balanced, while the layer height can be tuned to the property that dominates the application.

5.5 Comparison of the tri-fibre laminate with individual filaments

After optimisation, specimens of PETG-CF, ASA and PETG were printed individually under the same parameters and tested alongside the tri-fibre laminate. The peak values are listed in Table 9 and compared in Fig. 5. The tri-fibre laminate gave the highest compressive strength (26.41 N/mm², about 31 % above PETG-CF and 12 % above ASA) and the highest impact energy (3.43 J versus 3.17 J for PETG-CF), and its tensile strength (30.12 N/mm²) was within 5 % of PETG-CF (31.79 N/mm²). In flexure the laminate (0.29 kN) did not reach the value of PETG-CF (0.62 kN), reflecting the lower stiffness of the ASA and PETG stacks placed in the tension and compression faces of the bend specimen. Overall the multi-material laminate combines the toughness of PETG with the strength of PETG-CF and the compressive performance of ASA, and its mechanical behaviour was satisfactory relative to every individual filament.

Table 9. Peak mechanical properties of the tri-fibre laminate and individual filaments

Property	Tri-fibre	PETG-CF	ASA	PETG
Tensile strength (N/mm²)	30.12	31.79	21.03	0.94
Compressive strength (N/mm²)	26.41	20.14	23.48	14.02
Flexural load (kN)	0.29	0.62	0.22	0.36
Impact energy (J)	3.43	3.17	2.94	3.04

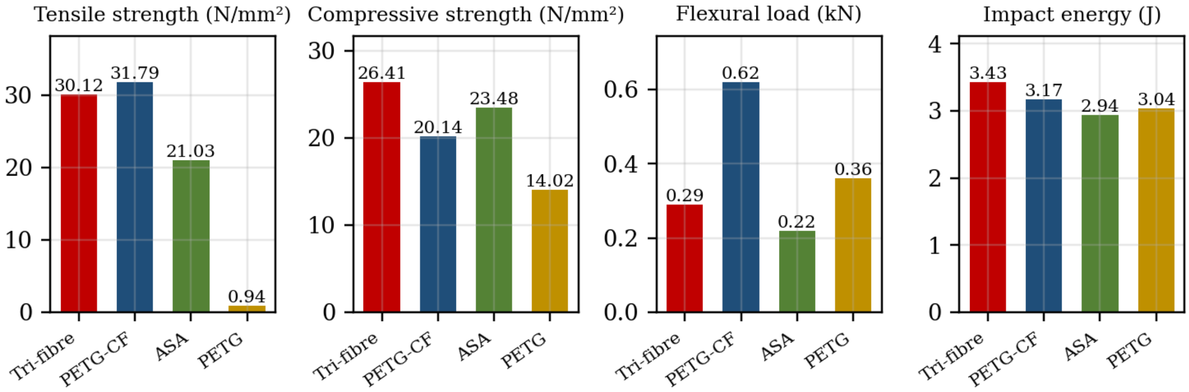

Fig. 5. Comparison of peak mechanical properties of the tri-fibre laminate with PETG-CF, ASA and PETG

VI. CONCLUSION

A five-nozzle FDM printer was developed and used to fabricate tri-fibre PETG-CF/ASA/PETG laminates, whose mechanical behaviour was optimised with a Taguchi L9 design over layer height, printing speed and infill density. The main conclusions are:

1. Printing speed is the most influential parameter, contributing 56 % of the variation in tensile strength and 48 % in compressive strength; layer height dominates impact energy (49 %). Infill density matters only for compressive strength (27 %). Flexural load is insensitive to the chosen process window and is governed by the laminate stacking and the carbon-fibre fraction.
2. The optimum settings are 0.30 mm / 70 mm/s / 30 % for impact energy (≈ 3.45 J) and compressive strength (≈ 26.9 N/mm²), and 0.15 mm / 70 mm/s / 20 % for tensile strength (≈ 31.0 N/mm²). A high printing speed with high infill is beneficial for all strength responses.
3. Peak tensile strength is obtained when the PETG fraction of the laminate is largest, whereas peak compressive strength and flexural load correspond to the largest ASA fraction; the highest impact energy is obtained with the thickest layers and a large PETG-CF fraction.
4. The tri-fibre laminate outperformed all individual filaments in compressive strength (26.41 N/mm²) and impact energy (3.43 J), nearly matched PETG-CF in tensile strength and fell short of PETG-CF only in flexural load.
5. Because the L9 design leaves only two error degrees of freedom, none of the factors is statistically significant at the 5 % level; replicated confirmation experiments at the identified optima, and extension of the design to nozzle temperature and layer sequence, are recommended as future work.

ACKNOWLEDGMENT

The authors thank the faculty and technical staff of the Department of Mechanical Engineering, NITTTR Chennai, for providing the 3D printing and mechanical testing facilities used in this work.

REFERENCES

[1] H. Kim et al., "Experimental study on mechanical properties of single- and dual-material 3D printed products," Procedia Manufacturing, vol. 10, pp. 887–897, 2017.

[2] S. H. Arigela and Vikram Kumar Ch R, "Investigation on dual nozzle fused deposition modelling using industrial robot," Advances in Materials and Processing Technologies, 2020, doi: 10.1080/2374068X.2020.1855400.

[3] V. Daramwar and S. Kadam, "Design and development of multi-material extrusion in FDM 3D printers," vol. 7, no. 3, Mar. 2020.

[4] J. Giri, P. Shahane, S. Jachak, R. Chadge and P. Giri, "Optimization of FDM process parameters for dual extruder 3D printer using artificial neural network," Materials Today: Proceedings, vol. 43, pp. 3242–3249, 2021.

[5] G. Issayev, "Bonding strength analysis of multi-material and multi-color specimens printed with multi-extrusion printer," Manufacturing Technology, 2021, doi: 10.21062/mft.2021.072.

[6] Sunil Kumar K, "Design and development of dual extruder 3D printer," vol. 3, no. 2, Aug. 2023.

[7] F. Shojaie, C. Ferrero and I. Caraballo, "Development of 3D-printed bicompartmental devices by dual-nozzle fused deposition modeling (FDM) for colon-specific drug delivery," Pharmaceutics, vol. 15, p. 2362, 2023, doi: 10.3390/pharmaceutics15092362.

[8] M. Szczęch and W. Sikora, "The influence of printing parameters on leakage and strength of fused deposition modelling 3D printed parts," Advances in Science and Technology Research Journal, vol. 18, no. 1, pp. 195–201, 2024, doi: 10.12913/22998624/178330.

[9] A. Wang, X. Tang, Y. Zeng, L. Zou, F. Bai and C. Chen, "Carbon fiber-reinforced PLA composite for fused deposition modeling 3D printing," Polymers, vol. 16, p. 2135, 2024, doi: 10.3390/polym16152135.

[10] R. Alkabbanie, B. Aktas, G. Demircan and S. Yalcin, "Short carbon fiber-reinforced PLA composites: influence of 3D-printing parameters on the mechanical and structural properties," Iranian Polymer Journal, vol. 33, pp. 1065–1074, 2024, doi: 10.1007/s13726-024-01315-8.

[11] M. Kaushik, V. R. Srinivasan and C. P. S. Prakash, "Experimental investigation of 3D printing on PLA reinforced with CF using FDM process," vol. 7, special issue 5, June 2022, doi: 10.56452/Jun_99.

[12] G. J. Pérez Mendoza, H. Y. Hernández Acosta and A. Miranda Cid, "Mechanical properties of PLA with CF printed at 40%, 80% and 100% infill percentages," Microscopy and Microanalysis, vol. 29, suppl. 1, pp. 1447–1449, 2023, doi: 10.1093/micmic/ozad067.744.

[13] H. Li, L. Liang, W. Zeng, Y. Deng, N. Ge and W. Shan, "3D printing polyurethane acrylate (PUA) based elastomer and its mechanical behavior," Materials Research Express, vol. 10, p. 055306, 2023, doi: 10.1088/2053-1591/acd740.